

Determination of normal and shear residual stresses from fracture surface mismatch

Araujo de Oliveira, J. , Kowal, J. , Gungor, S. and Fitzpatrick, M.E.

Author post-print (accepted) deposited in CURVE June 2016

Original citation & hyperlink:

Araujo de Oliveira, J. , Kowal, J. , Gungor, S. and Fitzpatrick, M.E. (2015) Determination of normal and shear residual stresses from fracture surface mismatch. Materials & Design, volume 83 : 176-184.

<http://dx.doi.org/10.1016/j.matdes.2015.06.014>

Publisher statement: NOTICE: this is the author's version of a work that was accepted for publication in Materials & Design. Changes resulting from the publishing process, such as peer review, editing, corrections, structural formatting, and other quality control mechanisms may not be reflected in this document. Changes may have been made to this work since it was submitted for publication. A definitive version was subsequently published in Materials & Design [Vol 83 (2015)]. DOI: 10.1016/j.matdes.2015.06.014.

© 2015, Elsevier. Licensed under the Creative Commons Attribution-NonCommercial-NoDerivatives 4.0 International <http://creativecommons.org/licenses/by-nc-nd/4.0/>

This document is the author's post-print version, incorporating any revisions agreed during the peer-review process. Some differences between the published version and this version may remain and you are advised to consult the published version if you wish to cite from it.

CURVE is the Institutional Repository for Coventry University
<http://curve.coventry.ac.uk/open>

Determination of normal and shear residual stresses from fracture surface mismatch

J. Araujo de Oliveira^{a,*}, J. Kowal^a, S. Gungor^a, M. E. Fitzpatrick^b

^a*Materials Engineering, The Open University, Walton Hall, Milton Keynes MK7 6AA*

^b*Now at: Faculty of Engineering and Computing, Coventry University, Priory Street, Coventry CV1 5FB, UK*

Abstract

The contour method of residual stress measurement has recently been adapted to measure fractured, rather than cut specimens. The fracture contour method was capable of determining normal residual stresses acting prior to the plane-strain failure of a large aluminium alloy forging, but shear residual stresses could not be measured (Prime *et al.*, 2014, Eng. Fract. Mech., 116, 158-171).

We demonstrate that the application of digital image correlation to topographic measurements of a fracture surface pair allows the determination of shear residual stresses in addition to the normal stress component. Miniature compact tension samples were extracted at an angle from a bent beam to give a known variation in normal and shear residual stress on the fracture plane. The material used was a metal matrix composite, which could be deformed plastically to introduce a known distribution of stresses and also present limited plasticity upon fracture, allowing plane-strain condition in a small specimen. The samples were fractured at cryogenic temperatures to further restrict plasticity. Although the fracture surface was non-planar and evidence suggested the occurrence of plasticity near the edges, experimental results correlated fairly well with the calculated normal and shear residual stress profiles.

Keywords: Residual stress, Fracture, Contour method, Digital Image Correlation, Shear stress

*Corresponding author - Tel: +44 1908 653 452 - Email: jeferson.oliveira@open.ac.uk

1. Introduction

Long-range residual stresses (type I or macrostresses) may lead to distortions or even premature failure of engineering components during manufacture or in service [1, 2]. Therefore the measurement of these stresses, which are dependent on the thermal, chemical and mechanical history of the component, is an important step in materials characterization. Residual stresses are usually measured by diffraction techniques, using either neutrons or X-rays, or by relaxation methods, such as hole drilling, slitting [1, 2] and the contour method [3]. However, the recently demonstrated fracture contour method [4] is currently the only technique capable of retrieving residual stress information after the unexpected failure of engineering components.

In principle, after an ideal brittle (elastic) fracture, in the absence of residual stresses, the two fractured halves should mate together perfectly. However, when a specimen containing residual stresses is fractured, these stresses are relaxed, causing a misfit of the topographical features on the fracture surfaces. The residual stress component acting normal to the surface can be obtained from the measurement of these misfits, as explained in detail by Prime *et al.* [4]. As usual in residual stress relaxation techniques, the method assumes elasticity, *i.e.* the fracture process does not induce significant levels of plasticity, and an additional assumption is that no material detaches from the surfaces upon failure. Despite these limitations, this unique method has the potential to become an important tool in failure analysis. This is especially true when the thermo-mechanical history of a component that failed in service is unknown or cannot be replicated, meaning that no other technique can be used to evaluate the residual stresses formerly present in that component.

In their article, Prime *et al.* [4] present the method to determine the residual stresses normal to the fracture surface (σ_{xx}). However, when a specimen containing residual stresses is fractured, not only one, but three residual stress components formerly acting on the fracture surfaces are fully relaxed – the one normal to the surface (σ_{xx}) and two shear components (τ_{xy} and τ_{xz}) – all of

which, contribute to the misfit of the fracture surface features. Therefore, in theory, these shear stresses can also be determined using the fracture contour method based on the in-plane misfits [3], but this has not yet been demonstrated in practice. Note that the other components of the residual stress tensor (σ_{yy} , σ_{zz} and τ_{yz}) are partially relaxed by the fracture, but their contribution to the misfit is negligible [4].

Methods have been reported to measure multiple residual stress components using the contour method. They use either a combination of multiple experimental methods [5, 6, 7] or multiple contour cuts [8, 9, 10]. By performing additional measurements on a contour cut specimen using, for example, X-ray diffraction, hole-drilling or slitting (multiple methods), it is possible to reconstruct the residual stress components that are partially relaxed by the cut in addition to the fully relaxed normal component [5, 6, 7]. However, this does not allow the measurement of the shear stress components that are fully relaxed. In fact, with multiple methods it is assumed that these shear stresses are negligible; otherwise multiple solutions to the stress state would be possible. By performing a series of contour cuts (multiple cuts), multiple (generally orthogonal) stress components can be determined [10]: without additional assumptions about the residual stress field, it is not possible to determine the shear residual stresses that are fully relaxed by the cuts. If additional assumptions about the residual stress field can be made (*e.g.* in a continuously-processed body), the complete residual stress tensor can be determined [8, 9].

The technique presented here is capable of determining 2-D maps of the fully relaxed normal and shear stress components without additional assumptions about the residual stress field and all the information is acquired from a single pair of fracture surface topography profiles.

Being able to determine three residual stress components by simply measuring the topography of a fracture surface pair could be particularly useful in forensic analysis of non-stress-relieved components, *e.g.* welded, heat treated or parts with complex geometry. Plane-strain fractures generally occur normal to the principal direction of the total stress, *i.e.* the superposition of applied and

residual stresses. These two sources of stress may present different principal directions. In these cases, in order to fully understand the role of residual stresses in the failure, it is important to measure the normal and shear residual stresses
65 that were acting on the fracture path prior to the failure.

Since the rough fracture surfaces have recognisable mating features, the in-plane misfits caused by the relaxation of the shear stresses could possibly be determined by a technique with the following characteristics:

- non-contact, in order to preserve fragile features on the surfaces;
- 70 • full-field, that is, to be able to resolve 2-dimensional sets of displacements;
- provide micron-level resolution, which is required for determination of typical residual stress fields in most engineering components;
- acquire the required data from a set of rough fracture surface;
- track the surface features without the need to modify the surface, such as
75 the introduction of speckle patterns;
- take one fractured half as reference and track the misfit based on the other fractured half.

Two-dimensional digital image correlation (DIC) [11] is a data analysis technique capable of resolving 2-D maps of in-plane displacements. It is usually
80 applied to images of a single specimen in two or more stressed states. With this method, the digital image from the reference state of the workpiece is divided into pre-defined subsets of pixels, which are then searched for in the corresponding image of the workpiece in the state to be measured (the measurement image). In-plane displacement vectors (v and w) are calculated from the difference in
85 position between the original location of the subset in the reference image and the place in the measurement image where the best correlation is found.

Because it uses digital images, DIC is usually non-contact and can cover a wide range of resolutions, depending mainly on the equipment used for the image acquisition. Using pattern matching algorithms, it is possible to resolve

90 displacements much smaller than the pixel dimensions in the image [11]. Evidence suggests that DIC would be able to correlate rough fracture surfaces without any additional modification. It has been applied to images from atomic force microscopes (AFM) [12], which are, generally, topography measurements. Since digital images based on topographic profiles are not directly affected by
95 differences in surface illumination – the greyscale in the images relate solely to the out-of-plane positions – the technique is able to correlate topographic profiles from the two fractured halves, as explained in Section 3.

The fracture contour method is still in its infancy: we believe that we are only the second team worldwide to apply it and that the proposed method for
100 extracting shear residual stress is entirely novel. It is still unknown how small the fractured specimen can be for the technique to be still able to retrieve the residual stress information. To date, only two articles describing the application of the method have been published. One reports the measurement in a nearly-ideal specimen: a large 7050 aluminium alloy forging, with a $209 \times 207 \text{ mm}^2$
105 cross-section, which is less prone to plastic deformation upon failure and in which the measured fracture surface misfit is relatively large (in the range of about $600 \mu\text{m}$). It is important to note that the fracture was not brittle, but the effect of plastic deformation was negligible due to the large size of the specimen. It is still mentioned that the signal to noise ratio was approximately 10:1, meaning
110 that misfits of about $60 \mu\text{m}$ could be determined [4]. In contrast, the other publication reports our unsuccessful application of the method to a fatigue crack followed by a plane-strain fracture with shear lips [13], in which the excessive plasticity that occurred upon failure prevented a successful result. Since the fracture contour method is still in its early development, it is important to
115 explore its applicability to the measurement of the residual stresses in specimens with cross-sections smaller than $10 \times 10 \text{ mm}^2$, which are representative of many engineering components. At this scale, the challenge is that common engineering materials present much lower ranges of fracture surface mismatch and are more prone to plastic deformations.

120 In this paper, a method is described to extend the application of the frac-

ture contour method to determine shear residual stresses in addition to the currently-measured normal stress component. The measurement was performed in a miniature compact tension specimen extracted from a bar of composite material in which a known residual stress distribution had previously been introduced. The specimen extracted from this bar was designed to have significant shear stresses in the plane of fracture. This was done by plastically deforming the bar in a four-point bending fixture and then extracting the sample at an angle relative to the principal stress direction, as shown in Figure 1. The miniature specimen extracted from the bent bar was then fractured in plane-strain condition and the topography of the fracture surfaces was measured. The out-of-plane misfits were determined by averaging the topography of the two fractured halves as in the current method [4]. In addition, the topographical profiles of the two fractured halves were converted into greyscale images to allow the determination of the in-plane misfits caused by shear stress relaxation using digital image correlation. The three sets of misfits (or displacements u , v and w) were then input as boundary conditions in a finite element model to calculate the normal and shear residual stresses that were present prior to the failure of the specimen. The experimental results were validated using finite element and analytical predictions of the residual stresses introduced by the four-point-bending test.

2. Materials

A bar with a nominal rectangular section of $24.5 \times 6 \text{ mm}^2$ and 140 mm length was extracted by wire electro-discharge machining (EDM) from a hot-forged plate of an aluminium metal matrix composite (XFINE225). The plate was manufactured by Materion UK (formerly Aerospace Metal Composites) by means of powder metallurgy via a proprietary process comprising high energy mixing, hot isostatic pressing and hot forging. The composite is an aluminium alloy AA2124 matrix reinforced with 25 vol.% (29.4 wt.%) of silicon carbide particles. The nominal diameter of the particles is $0.7 \text{ }\mu\text{m}$. The parent plate

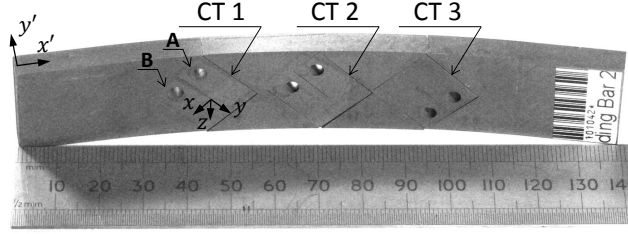


Figure 1: Photograph of the bent bar, showing the location and orientation at which the compact tension specimen number 1 (CT 1), the object of this study, was extracted.

150 was air cooled from forging; hence low residual stresses were expected. Contour method measurements were performed in the parent plate from which the bar was extracted, confirming that stresses were within ± 5 MPa over most of the cut face, being reasonable to assume that the extracted bar was initially free of residual stresses.

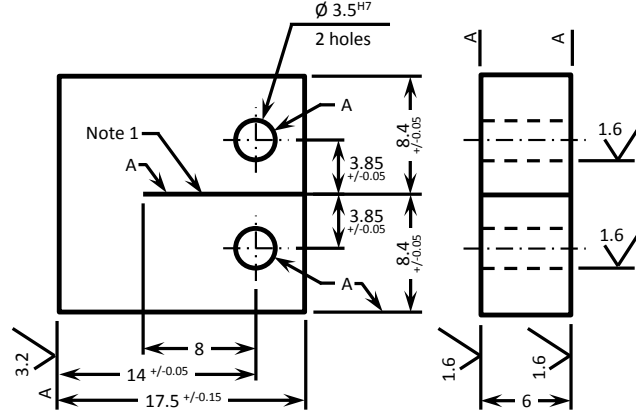
155 The composite bar was plastically bent in order to introduce a uniaxial residual stress field. A four-point bending fixture, with outer and inner spans of 120 and 90 mm respectively, was mounted on an Instron 3367 frame with an Instron 2530-444 load cell rated to ± 30 kN. The assembly was loaded to 19.6 kN at a displacement rate of $0.11 \text{ mm} \cdot \text{min}^{-1}$.

160 Standard compact tension (C(T)) samples with a width W of 14 mm [14] (see Figure 2) were extracted by wire EDM from the plastically bent bar in a region between the inner rollers, where a uniform longitudinal residual stress field was expected, at an angle of 45° relative to the longitudinal direction of the bar, as shown in Figure 1. By doing this, the plane where the sample was
165 expected to fracture should contain the highest shear residual stress variation.

3. Methods

3.1. Analytical calculation of the residual stresses

The through-thickness distribution of residual stress introduced by pure bending in a rectangular section beam was first calculated using an analytical method. The calculation was based on the tensile stress-strain behaviour of
170



Note 1 – Wire EDM notch made using $\varnothing 0.1$ mm wire.

Figure 2: Schematic showing the dimensions of the C(T) specimen according to the A.S.T.M. standard E399-12ε1 [14]

the material and the measured radius of curvature of the region subject to pure bending as described below. This approach was used owing to the failure of the strain gauges mounted on the sample during the actual four-point bending test. Note that this calculation was initially performed based on the x' - y' coordinate system and then rotated to match the coordinate system of the extracted specimen, x - y - z (both shown in Figure 1).

It was assumed that the pure bending produced a uniaxial stress state and that the material was homogeneous, isotropic [15] and had the same stress-strain behaviour under tension and compression (which is discussed in Section 5).

Based on the assumptions above, the longitudinal strain $\epsilon_{x'}$ at a distance y' from the neutral surface - *i.e.* the position through the thickness of the beam where $\epsilon_{x'}$ and $\sigma_{x'}$ are zero - could be determined using Equation 1 [16], where c is the distance from the neutral surface to the convex face of the beam and ϵ_m is the longitudinal strain in that same face, as illustrated in Figure 3.

$$\epsilon_{x'} = \frac{\epsilon_m}{c y'} \quad (1)$$

Since it is assumed that the material behaves similarly under tension and

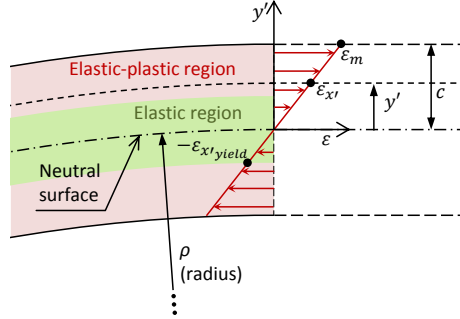


Figure 3: Diagram showing the model of longitudinal strain distribution of a specimen with a rectangular cross-section loaded in pure bending.

compression, c is equal to one half of the thickness of the bar and the tensile stress-strain curve of the material can be mirrored to describe the compressive and tensile stress-strain behaviour of the material ($\sigma_x(\epsilon_x)$), shown in Figure 4 (a).

190 Then, if ϵ_m is known, the longitudinal stress as a function of the distance from the neutral surface, $\sigma_{x'} = f(y')$, can be obtained by combining the stress-strain curve with Equation 1. However, since in the actual experiment the strain gauges attached to the convex and concave faces of the specimen unexpectedly failed long before the maximum load was reached, ϵ_m was still unknown. Therefore, using Equation 1, the stress as a function of position through thickness still
 195 had ϵ_m as a parameter, giving $\sigma_{x'} = f(\epsilon_m, y')$.

To enable the determination of ϵ_m , the radius of curvature of the neutral surface of the unloaded bent beam (ρ) in the region between the two inner rollers of the four-point bending fixture was measured. In the elastic regime, ρ relates
 200 to the longitudinal strain ($\epsilon_{x'}$) and to the distance from the neutral surface (y') according to Equation 2 [16].

$$\rho = \frac{y'}{\epsilon_{x'}} \quad (2)$$

Wherever the longitudinal stress ($\sigma_{x'}$) does not exceed the yield stress of the material during loading, the elastic regime is still valid in the bent residually

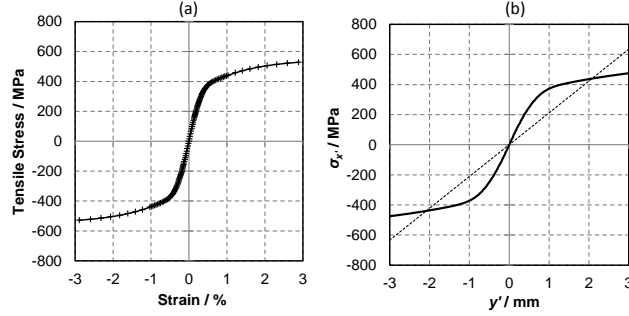


Figure 4: Plots of (a) the mirrored tensile stress-strain curve of the material, representing $\sigma_x(\epsilon_{x'})$; and (b) the applied stress distribution as a function of through-thickness position ($\sigma_{x'}(y')$) at maximum applied bending load, also showing the dashed line representing the elastic relaxation needed for the profile to reach equilibrium, which was used to analytically calculate the residual stresses distribution.

stressed sample. Based on that, an iterative method was used in order to calcu-
 205 late a residual stress field that would result in the measured curvature. Using the
 model, an estimated ϵ_m would give a certain applied stress distribution, which
 was then elastically relieved to reach force and moment equilibrium in order to
 reveal the through-thickness distribution of longitudinal residual stress. From
 this residual stress profile, a point where the beam had only deformed elasti-
 210 cally, based on the calculated applied stress distribution (see Figure 4 (b)), was
 used to calculate the expected radius of curvature using Equation 2. If the cal-
 culated radius was lower than the one measured in practice, ϵ_m was increased
 and vice versa until the calculated and measured radii were equal, resulting in
 the through-thickness longitudinal residual stresses distribution, $\sigma_{x'}(y')$.

215 Since the C(T) sample was extracted at 45° in relation to the principal di-
 rection of the bent bar (x'), Mohr's circle [16] was used to determine the normal
 and shear stresses in the region where the C(T) specimen was expected to frac-
 ture, so that the resulting stress tensor had as reference the x - y - z coordinate
 system presented in Figure 1. It is important to note that any partial relax-
 220 ation of residual stresses owing to the extraction of the C(T) sample was not
 considered in the analytical solution.

3.2. Finite element analysis

The residual stresses in the C(T) samples were also predicted using Abaqus v6.11 finite element code. A 3-D quasi-static non-linear finite element model of a bar matching the geometry and the tabular true tensile elastic-plastic behaviour of the particle-reinforced aluminium composite was meshed with 73,160 eight-noded first-order elements with reduced integration and hourglass control (C3D8R). The model included four analytical rigid rollers matching the configuration of the four-point bending apparatus, which transferred to the modelled bar the same load as was measured in the experimental procedure, leading to a distribution of plastic deformations in the bar. In the following step, the bar was unloaded to reach stress equilibrium. After that, a predefined set of elements was excluded from the simulation, leaving activated only elements in the shape of a C(T) sample placed at an angle of 45° in relation to the longitudinal direction of the bent bar (simulating the extraction of the specimen labelled CT 1 shown in Figure 1), and a new stress equilibrium was calculated. The result was the expected residual stress distribution in the C(T) sample 1 as extracted, *i.e.* before it was fractured.

3.3. Experimental determination of residual stresses

The residually-stressed C(T) sample was fixed to an MTS811 servo-hydraulic test frame and then cooled to -120°C in an Instron 3119-407 environmental chamber in order to increase the yield strength and reduce the fracture toughness of the metal matrix alloy. It was then loaded in tension to rupture in a predominantly plane-strain condition, creating the fractured halves **A** and **B**. It is important to note that the intent of this test was simply to fracture the specimen in a brittle manner, since the fracture contour method assumes elasticity. Therefore, although notched C(T) samples are usually fatigue sharpened before rupture [14], this operation was not performed on this specimen, with the objective of reducing the amount of plasticity induced on the fracture plane. A photograph of the fractured specimen is shown in Figure 5.

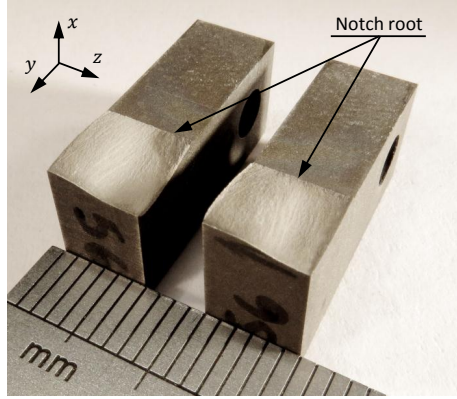


Figure 5: Photograph of sample CT 1 showing the brittle fracture surfaces. The ruler scale is in millimetres.

To allow the determination of the in- and out-of-plane displacements, the topography of fracture surfaces of both halves was measured using a Leica DCM 3-D confocal microscope with a pitch of $1.66\text{ }\mu\text{m}$ in both y and z directions in a sampled area of about 6.27 by 6.2 mm^2 . Owing to the limited field of view of the equipment, the area was divided into 48 frames, each with 767 by 565 measurement locations. The frames overlapped each other by $273.22\text{ }\mu\text{m}$ in y and $187.9\text{ }\mu\text{m}$ in z , totalling $20,801,040$ points measured. Note that stitching the surface profiles prior to the DIC analysis would lead to significant systematic errors in the in-plane displacement profiles; hence the results of the DIC analysis of each frame were stitched instead, reducing those errors to negligible levels.

To determine the in-plane displacements using DIC, the surface measurements were converted into 16-bit greyscale images, in which the y - z position of each point determined the pixel location and the height (x) determined its shade of grey value based on the x range within each frame. Note that the frames from the measurement of the half **B** were rotated 180° about the y axis before the conversion, resulting in a set of 48 pairs of images, each corresponding to a particular region from the fracture faces. Each pair of images was correlated using commercial DIC software, LaVision Davis 8.2.1. An example of a correlated pair of frames is shown in Figure 6. Five iterations of 2-D deformation

calculation were performed with a subset size of 128 by 128 pixels and 50% of
 overlap. After that, nine iterations with a refined grid of 32 by 32 pixel subsets
 with an overlap of 75% were performed. A post processing step was carried out
 in order to eliminate results with a low correlation factor and those that did
 not follow the overall trend. The 48 sets of results were then stitched together,
 giving y - z maps of displacements in y and z directions, respectively v and w
 (see figures 7 (b) and (c) as well as figures 8 (b) and (c)). It is important to
 note that, at this point, these displacements have as reference an arbitrary co-
 ordinate system. However, as explained by Prime *et al.* [4], at the modelling
 stage of the fracture contour method this arbitrary coordinate system does not
 affect the residual stress measurement, as it contributes only to rigid body mo-
 tion of the model. Another important note is that the displacements measured
 with DIC are the in-plane difference in the position of the features between the
 two fracture surfaces; but for the fracture contour method, the displacements
 should go from one fractured half to the position of equilibrium [4]. Therefore,
 the in-plane displacement magnitudes were divided by two, taking advantage of
 the symmetry between the two fractured halves.

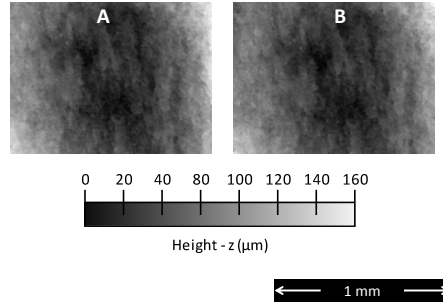


Figure 6: Example of frames obtained from the topography of the fracture surfaces of halves **A** (left) and **B** (right) ready for the digital image correlation.

To retrieve the displacements relative to the normal residual stress relaxation
 (u), the point density of the frames from the half **A** was reduced by filtering
 out 14 out of every 15 points in y and z directions in order to reduce the compu-
 tation time required to perform the subsequent operations. Before reducing the

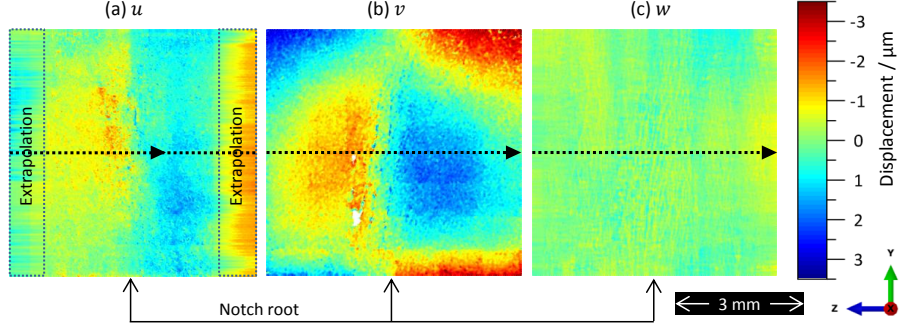


Figure 7: Maps of normal displacements u (a), obtained by averaging the topography of both fractured halves as well as in-plane displacements v (b) and w (c) obtained from DIC.

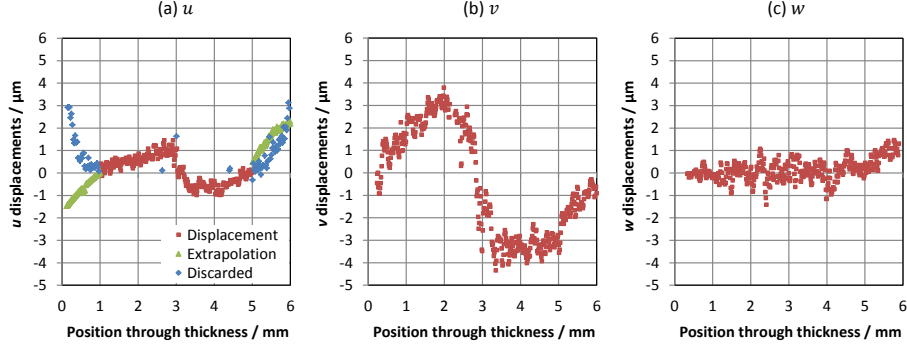


Figure 8: Line profiles of normal displacements u (a), obtained by averaging the topography of both fractured halves as well as in-plane displacements v (b) and w (c) obtained from DIC along the dotted lines shown in Figure 7.

point density of the half **B**, each measured frame from this half was aligned to the half **A** by translating it in y and z using the displacements resolved by DIC. The points from the half **B** were only filtered after alignment was performed. Finally the x coordinates of both halves at each y - z position were averaged, as normally done in (fracture) contour method measurements, resulting in the out-of-plane displacements, u , presented in figures 7 (a) and 8 (a). Evidence suggests that the occurrence of plasticity near the edges of the sample had a detrimental effect on the normal displacements, which is discussed in more detail later. Therefore, normal displacements near the edges were not included in

300 the analysis, but the displacements in those regions were extrapolated using second order splines to result in a set of displacements containing the information about the relaxation of the normal residual stress component.

The three displacement maps (the normal, u , as just described and the in-plane from DIC, v and w) were smoothed using bi-quadratic splines with
305 1 mm node spacing. The smoothed displacements u , v and w had their sign reversed and were applied one by one as boundary conditions on the surface nodes of a linear-elastic 3-D finite element model of one half of the C(T) sample in order to calculate the normal and shear residual stresses that were present prior to the failure. The reason for applying the displacements one by one
310 is discussed later. The model was created using Abaqus v6.11 and the part was meshed using 8-noded first-order elements with reduced integration and hourglass control (C3D8R). The Young's Modulus and Poisson's ratio of the composite (115 GPa and 0.3 respectively, given by the supplier) were used in the calculations. Note that in each step of the simulation it is necessary to
315 include additional nodal constraints against rigid body motion [4].

4. Results

The map of normal residual stresses from the fracture contour method presented in Figure 9 (d) is in fairly good agreement with the finite element model predictions (Figure 9 (a)), although near the edges the agreement is not as good.
320 The positions of the regions with compression and tension, as well as regions where the normal residual stress is zero, correlate reasonably well with the finite element prediction, although the peak magnitudes in the experimental results are higher than predicted.

Observations are similar when comparing the maps of the τ_{xy} component of
325 residual stresses determined by the fracture contour method with the finite element model predictions, as shown respectively in figures 9 (e) and (b), although near the edges the results are worse than for the normal component. Predictions and measurements of the τ_{xz} component of residual stresses, presented

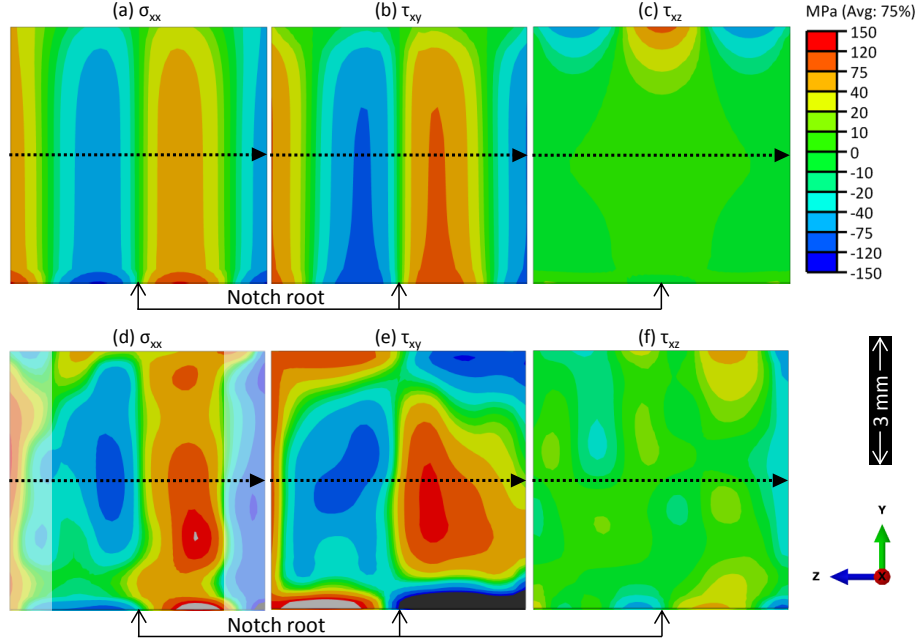


Figure 9: Finite element prediction of the residual stress components (a) σ_{xx} , (b) τ_{xy} and (c) τ_{xz} as well as experimental results of the same components (d) σ_{xx} , (e) τ_{xy} and (f) τ_{xz} obtained from the fracture contour method combined with the digital image correlation technique, with the displacements being applied individually as boundary conditions on the surface nodes of the finite element model. Regions based on extrapolation are shown faded.

respectively in figures 9 (c) and (f), show good overall agreement.

Figure 10 (a) shows the through-thickness distribution of the normal residual stresses, along the paths shown as dotted lines in figures 9 (a) and (d), including analytical, finite element and experimental results. Note that the experimental results are shown faded in the region where the displacements were extrapolated (rather than directly measured). This plot confirms the observations made in the contour maps, although it can be noted that not all the positions where experimental results cross the horizontal axis coincide with the analytical and finite element predictions. Another noticeable feature is that the normal residual stress peak values in the analytical solutions are higher than the peaks in the finite element predictions.

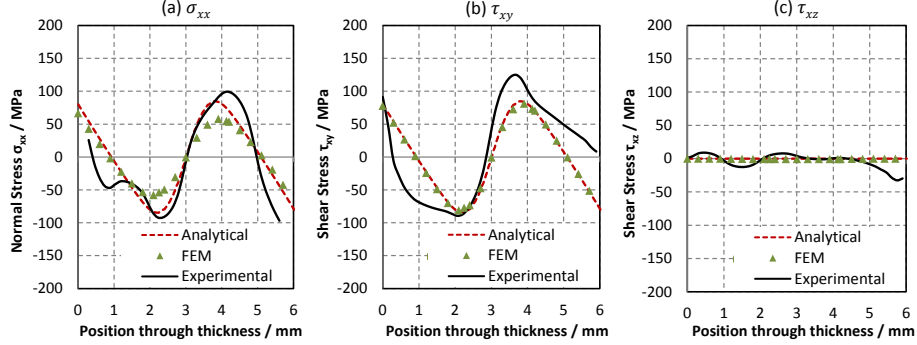


Figure 10: Through-thickness distributions ($-z$ sense) of (a) normal, σ_{xx} and shear, (b) τ_{xy} and (c) τ_{xz} residual stress components showing a comparison of analytical, finite element and experimental results along the dotted lines shown in Figure 9.

340 Similarly, line profiles along the dotted lines in Figure 9 (b) and (e) of the τ_{xy} component of residual stresses are shown in Figure 10 (b). It can be noted in this plot that, although the experimental results seem to reach stress balance, they would not reach moment balance – calculated by integrating (along the line) the shear force times the distance to the mid-thickness – as expected in this particular case. In addition, the trend of experimental results in the vicinity of the neutral surface (mid-thickness) is steeper than predicted. However, the trend of the measured residual stresses correlate fairly well with the analytical and finite element predictions, showing peaks nearly in the same position with similar magnitudes.

350 Figure 10 (c) shows the τ_{xz} distribution along the dotted lines in figures 9 (c) and (f), where experimental measurements correlate well with finite element and analytical results, showing negligible residual stress levels.

5. Discussion

The range in the displacements estimated by the finite element model was about $5 \mu\text{m}$ on a $6 \times 6 \text{ mm}^2$ surface. The information was extracted from a surface with average roughness (R_a) of $24.8 \mu\text{m}$. The previous successful application of the fracture contour method was based on a range in displacements

over 100 times larger [4]. Although challenging, normal and shear residual stress measurements performed using a combination of the fracture contour method
360 with digital image correlation showed fairly good agreement with analytical and finite element predictions. Some of the factors that might have contributed to the differences found between the predictions and the experimental measurement need further consideration.

It was assumed that the parent composite bar was free of stresses prior to
365 the bending test. This assumption was supported by contour method measurements in the plate from which the bar was cut, indicating that normal residual stresses were within ± 5 MPa over most of the cut face, which could be neglected. However, since the strain gauges failed during the four point bending test, there was no direct experimental evidence to support the assumption that the elastic-
370 plastic behaviour of the material was the same under tension and compression. If this assumption is false, this would lead to errors. The metal matrix composite used in this study generally contains intergranular microstresses between the deformable aluminium alloy and the brittle silicon carbide particles because the composite is cooled down after production and the coefficients of thermal
375 expansion of the two materials are different [15, 17, 18]. These microstresses could potentially have an effect on the actual magnitude and position of the peak residual stresses introduced in the bending test, as they are relaxed by plastic deformation, and can even change sign for large deformations [19].

The displacements relative to the normal residual stress relaxation (x -direction)
380 tion) showed some signs of plasticity, hence the affected region was replaced by spline extrapolation - regions highlighted in Figure 7 (a). On the other hand, the in-plane displacements did not show clear signs of plasticity and were used in full. To verify the occurrence of plasticity, a sample with the same dimensions and material which was free of residual stresses was fractured and analysed
385 using the same method. Figure 11 shows the distribution of normal displacements - in the same location as the dotted lines in Figure 9 - extracted from the residually-stressed specimen as well as from the stress-free sample for comparison. According to the fracture contour method theory [4], if no plasticity

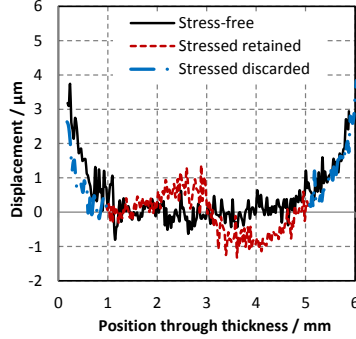


Figure 11: Distribution of normal displacements acquired from a residual-stress-free specimen as well as from the residually-stressed sample, highlighting the regions where measurements were discarded and replaced by spline extrapolations due to the evidence of plastic deformation near the sample surfaces.

occurs, the displacements from a stress-free sample would be a flat plane (or a
 390 straight line in a 2-D plot). However, Figure 11 suggests that plastic deformation
 occurred in the vicinity of the edges, which would have a detrimental effect
 in the residual stress determination. The region where data from the residu-
 ally stressed specimen was discarded and replaced with spline extrapolation is
 highlighted in Figure 11 and coincides well with the region where the results
 395 from the stress-free sample depart from a straight line, supporting the use of
 the extrapolated data over the actual measured displacements.

As presented before, the experimental measurements of the τ_{xy} residual
 stress component plotted in Figure 10 (b) do not seem to reach moment balance
 through the thickness, although balance was predicted by analytical and finite
 400 element methods. This means that this net moment is counter-balanced else-
 where on the plane of interest, since the residual stresses must balance over the
 fractured area. It can be noted in the residual stress map shown in Figure 9 (e)
 that the moment in the region of the dotted line is counter-balanced by the
 stresses near the notch root and the opposite edge. However, the stresses near
 405 these edges are susceptible to errors caused by a combination of plasticity upon
 fracture, noise in the digital image correlation measurements, and smoothing

artefacts. Since reasonable results were found near the side edges, it seems more likely that the imbalance was caused by plasticity, which is also supported by the evidence described above.

410 An interesting finding is that when each displacement map is individually applied as boundary conditions in the finite element model, instead of constraining all three directions simultaneously, the resulting stresses are slightly different. In fact, by comparing the results previously shown in Figure 9 with the maps obtained from the application of all displacements at the same time (shown in 415 Figure 12), it can be noted that all residual stress components are closer to the predictions when displacements are applied individually (figures 9 (c), (d) and (e)), while in theory, they were not expected to change. When the surface nodes are constrained in the three directions, any error or bias in the displacements map relative to one residual stress component will cause the error to propagate to the other stress components owing to the extra constraint. Evidence 420 for this is that the largest differences in the normal residual stress component noted between figures 9 (a) and 12 (a) are in the vicinity of the top and bottom edges, which are the locations where it seems that plasticity interfered with the τ_{xy} residual stress component.

425 Although less likely, another possible source for these differences is that the model used for calculating the stresses assumed a flat surface. The actual shape of the fracture surface, combined with having the three displacements applied simultaneously, could potentially have an impact in the determined stresses. This needs to be studied further. In the previous application of the fracture 430 contour method the fracture studied was in fact nearly flat and displacements were only applied in a single direction [4], which was not the case here.

Furthermore, the effect of uncertainties related to the DIC results was unlikely to be a major contributor to the observed difference for the following reasons:

- 435 • A series of filters was applied, as mentioned in Section 3, aiming to leave only high quality in-plane displacements to be used in the measurements.

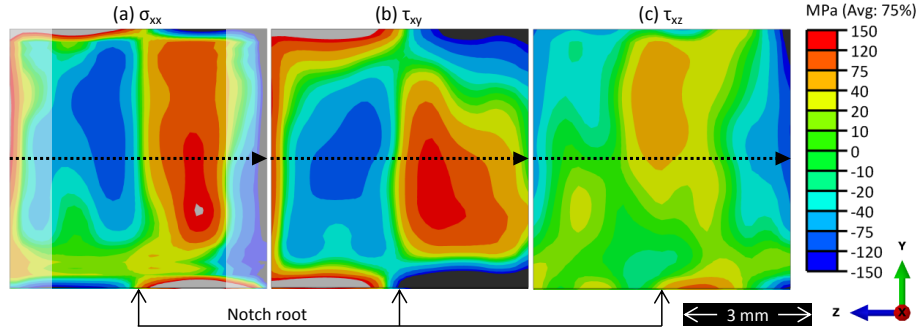


Figure 12: Experimental results of the residual stress components (a) σ_{xx} , (b) τ_{xy} and (c) τ_{xz} obtained from the fracture contour method combined with the digital image correlation technique, with the displacements being applied simultaneously as boundary conditions on the surface nodes of the finite element model. Regions based on extrapolation are shown faded.

- In addition, since the correlation was done frame by frame, if the uncertainty in DIC results or the stitching process were not satisfactory, the results from the entire surface would have been compromised, rather than being predominantly localised near the edges of the specimen, which was the case for the differences observed.
- The misalignment portion in the DIC results was consistent throughout the 48 correlated frames, as expected.

Owing to a combination of the high measurement density with the high sensitivity of DIC and the complex shape of the C(T) specimen extracted from the bent bar, a slight misalignment between halves **A** and **B** was observed in the DIC results, even though very careful alignment of the fractured halves was performed for the measurement of their topographies. However, as explained before, this misalignment only contributes to the rigid body motion of the model, having no noticeable effects on the residual stress determination. The DIC results were also used to align the two fracture topographies (frame by frame) before averaging them to calculate the normal displacements. This was crucial in mitigating the scatter due to the in-plane misalignment of the surface features caused by the relaxation of shear stresses. The scatter would be significant if

455 the topographies were simply aligned using the edges.

Finally, in larger specimens of similar materials, displacements of a greater range would be expected for the same residual stress levels, *e.g.* [4]. Furthermore, larger parts would be potentially less prone to plastic deformation upon plane-strain fracture, meaning that the method described here has the potential to measure normal and shear residual stresses with better accuracy in larger
460 parts. In addition, if suitable measurement methods are available, stresses in smaller parts made of more brittle materials could possibly be measured.

6. Conclusions

1. Normal and shear residual stresses have been measured in a compact tension specimen configuration using a combination of the fracture contour
465 method with the digital image correlation technique. The specimen was extracted from a bent bar to provide a variation in shear residual stress on the fracture plane.
2. The measured residual stresses show fairly good correlation with analytical
470 and finite element predictions, especially when displacements are applied individually as boundary conditions in the finite element model.
3. Evidence suggests that plasticity was the largest source of errors in the residual stress measurements, especially near the edges of the sample.
4. This technique enables the measurement of a 2-D map of three components
475 of the residual stress tensor that were present at the moment of failure in fractured specimens. This might be valuable in forensic analysis, as no alternative method currently exists that can yield this information.
5. The approach presented is expected to give better results in larger parts. Also, it might be applicable to the measurement of residual stresses in
480 smaller but more brittle parts, if suitable surface measurement equipment is available.
6. The effect of the shape of the fracture surface when displacements are applied in three orthogonal directions still needs to be evaluated, as a

non-planar fracture surface is a potential source of error in the final results.

485 7. Acknowledgements

We wish to thank Materion AMC for the provision of the material studied in the project. The authors are grateful for technical support from P. Ledgard, D. Flack, S. Hiller and A. Forsey at The Open University. JAO and MEF are supported by the Lloyd's Register Foundation (LRF), a UK registered charity that
490 helps to protect life and property by supporting engineering-related education, public engagement and the application of research.

References

- [1] P. J. Withers, H. K. D. H. Bhadeshia, Residual stress. Part 1 - Measurement techniques, *Materials Science and Technology* 17 (4) (2001) 355–365. doi:
495 10.1179/026708301101509980.
- [2] N. S. Rossini, M. Dassisti, K. Y. Benyounis, A. G. Olabi, Methods of measuring residual stresses in components, *Materials & Design* 35 (March) (2012) 572–588. doi:10.1016/j.matdes.2011.08.022.
- [3] M. B. Prime, Cross-sectional mapping of residual stresses by measuring the
500 surface contour after a cut, *Journal of Engineering Materials and Technology* 123 (2) (2001) 162–168. doi:10.1115/1.1345526.
- [4] M. B. Prime, A. T. DeWald, M. R. Hill, B. B. r. Clausen, T. Minh, M. Tran, Forensic determination of residual stresses and KI from fracture surface mismatch, *Engineering Fracture Mechanics* 116 (0) (2014) 158–171. doi:
505 10.1016/j.engfracmech.2013.12.008.
- [5] P. Pagliaro, M. B. Prime, J. S. Robinson, B. Clausen, H. Swenson, M. Steinzig, B. Zuccarello, Measuring Inaccessible Residual Stresses Using Multiple Methods and Superposition, *Experimental Mechanics* 51 (7) (2011) 1123–1134. doi:10.1007/s11340-010-9424-5.

- 510 [6] F. Hosseinzadeh, P. J. Bouchard, Mapping Multiple Components of the Residual Stress Tensor in a Large P91 Steel Pipe Girth Weld Using a Single Contour Cut, *Experimental Mechanics* 53 (2) (2013) 171–181. doi:10.1007/s11340-012-9627-z.
- [7] M. D. Olson, M. R. Hill, A New Mechanical Method for Biaxial Residual Stress Mapping, *Experimental Mechanics* (November 2014) (2015) 1–12. doi:10.1007/s11340-015-0013-5.
- 515 [8] A. T. DeWald, M. R. Hill, Multi-axial contour method for mapping residual stresses in continuously processed bodies, *Experimental Mechanics* 46 (4) (2006) 473–490. doi:10.1007/s11340-006-8446-5.
- [9] M. E. Kartal, C. D. M. Liljedahl, S. Gungor, L. Edwards, M. E. Fitzpatrick, Determination of the profile of the complete residual stress tensor in a VPPA weld using the multi-axial contour method, *Acta Materialia* 56 (16) (2008) 4417–4428. doi:http://dx.doi.org/10.1016/j.actamat.2008.05.007.
- 520 [10] P. Pagliaro, M. B. Prime, H. Swenson, B. Zuccarello, Measuring Multiple Residual-Stress Components using the Contour Method and Multiple Cuts, *Experimental Mechanics* 50 (2) (2010) 187–194. doi:10.1007/s11340-009-9280-3.
- [11] B. Pan, K. Qian, H. Xie, A. Asundi, P. Bing, Q. Kema, X. Huimin, A. Anand, Two-dimensional digital image correlation for in-plane displacement and strain measurement: a review, *Measurement Science and Technology* 20 (6) (2009) 62001. doi:10.1088/0957-0233/20/6/062001.
- 530 [12] S. W. Cho, J. F. Cardenas-Garcia, I. Chasiotis, Measurement of nanodisplacements and elastic properties of MEMS via the microscopic hole method, *Sensors and Actuators a-Physical* 120 (1) (2005) 163–171. doi:10.1016/j.sna.2004.11.028.
- 535

- [13] J. de Oliveira, M. E. Fitzpatrick, J. Kowal, Residual stress measurements on a metal matrix composite using the contour method with brittle fracture, in: *Advanced Materials Research*, Vol. 996, Trans Tech Publ, 2014, pp. 349–354. doi:10.4028/www.scientific.net/AMR.996.349.
- [14] ASTM-E399-12e1, Test Method for Linear-Elastic Plane-Strain Fracture Toughness K_{Ic} of Metallic Materials (2013). doi:10.1520/E0399-12E01.
- [15] M. E. Fitzpatrick, M. T. Hutchings, P. J. Withers, Separation of macroscopic, elastic mismatch and thermal expansion misfit stresses in metal matrix composite quenched plates from neutron diffraction measurements, *Acta Materialia* 45 (12) (1997) 4867–4876. doi:10.1016/S1359-6454(97)00209-7.
- [16] F. P. Beer, E. R. Johnston Jr., J. T. Dewolf, D. F. Mazurek, *MECHANICS OF MATERIALS*, sixth edit Edition, McGraw-Hill Education, 2010.
- [17] M. Kartal, F. Dunne, a.J. Wilkinson, Determination of the complete microscale residual stress tensor at a subsurface carbide particle in a single-crystal superalloy from free-surface EBSD, *Acta Materialia* 60 (2012) 5300–5310. doi:10.1016/j.actamat.2012.06.027.
- [18] M. Kartal, R. Kiwanuka, F. Dunne, Determination of sub-surface stresses at inclusions in single crystal superalloy using HR-EBSD, crystal plasticity and inverse eigenstrain analysis, *International Journal of Solids and Structures* (In press). doi:10.1016/j.ijsolstr.2015.02.023.
- [19] M. E. Fitzpatrick, P. J. Withers, A. Baczmanski, M. T. Hutchings, R. Levy, M. Ceretti, A. Lodini, Changes in the misfit stresses in an Al/SiCp metal matrix composite under plastic strain, *Acta Materialia* 50 (5) (2002) 1031–1040. doi:10.1016/S1359-6454(01)00401-3.